PHYSICAL REVIEW B VOLUME 23, NUMBER 10 15 MAY 1981

The s-d transition in compressed lanthanum

A. K. McMahan
Lawrence Livermore National Laboratory, University of California, Livermore, California 94550

H. L. Skriver
Research Establishment, Risö, DK-4000 Roskilde, Denmark
and Nordita, Blegdamsvej 17, DK-2100, Copenhagen, Denmark

B. Johansson
Section 214, Försvarets Forskningsanstalt, Avdelning 2, S-104 50 Stockholm, Sweden
(Received 28 October 1980)

Calculations of the pressure-volume isotherms for fcc La have been carried out up to pressures of 2 Mbars and temperatures up to 3.4 eV, using the self-consistent linear-muffin-tin-orbital method. The isothermal bulk modulus shows an anomalous stiffening over the pressure range 320–560 kbars, due to termination of the 6s to 5d electronic transition. The effect is calculated to be most pronounced at zero temperature and is largely washed out by a temperature of 3.4 eV. These results lead to a temperature-dependent peak in the lattice Grüneisen parameter, based on a simple Slater-model analysis. Hugoniot calculations using this Grüneisen parameter are in good agreement with experiment and reproduce the anomalous stiffening observed in the shock compression data for La. While we also find both significant overlap of the rare-gas cores and melting to occur in the vicinity of the shock anomaly, the present calculations identify the principal cause of the anomaly observed in the La shock data to be the termination of the 6s-5d electronic transition in this material.

I. INTRODUCTION AND CONCLUSIONS

We report self-consistent linear-muffin-tin-orbital[1] (LMTO) calculations of zero- and finite-temperature pressure-volume isotherms for fcc La, up to pressures of 2 Mbars and temperatures of 3.4 eV. The results show an anomalous stiffening in the bulk modulus of the static lattice over the pressure range 320–560 kbars, arising from termination of the 6s to 5d electronic transition. The effect is most pronounced at zero temperature and diminishes rapidly with increasing temperature, as is to be expected for an electronic transition anomaly. When these results are combined with a simple Slater model[2] for the nuclear Grüneisen parameter, the shock compression curve, or Hugoniot, may be calculated. Results of these calculations are in good agreement with experiment and indicate strongly that the primary cause of the anomaly seen in the experimental shock compression data for La is termination of the 6s-5d electronic transition.

The shock compression data for most of the rare earths displays an anomaly at about 40% compression, which appears as an abrupt change of slope in a plot of shock velocity versus particle velocity.[3-6] Proposed explanations have focused on three interrelated issues: (i) termination of the 6s-5d electronic transition,[4] (ii) overlap of the Xe cores,[5] and (iii) melting.[6,7] The f electrons do not appear to play a crucial role, as the 4f band lies initially above the Fermi level for La, or more important, the shock anomaly is also exhibited by other group-3A elements[4-6] (Sc, Y) for which there are no nearby f levels at all. The fact that the anomaly takes place at roughly the same volume contraction for all the trivalent rare earths also seems to show the non-involvement of the f electrons. The low-pressure phase of the rare earths, i.e., below the anomaly, is unusual in its own right, characterized by very low bulk moduli and Grüneisen parameters, reminiscent of the electronic transition induced softening which has been discussed for Cs.[8-10] (The bulk modulus of Cs is also unusually low even when compared to the other alkali metals.[11]) When the bottom of the 6s band rises above the Fermi level with compression, such a softening effect will terminate, which could lead to the observed stiffening. On the other hand, it has also been demonstrated that the near-neighbor distance at which the abrupt stiffening occurs coincides closely with calculations of the appropriate rare-gas core diameters.[5] Thus core repulsion might also explain the shock anomaly. The melting explanation[6,7] is based on the assumption that the electronic transition is farther along in the liquid, so that the solid transforms to a relatively stiffer liquid phase.

All three explanations are potentially related. Band-structure calculations show, in agreement with expectations from a simple application of Wigner-Seitz boundary conditions,[12] that the broadening of s and p core bands with compression

is generally accompanied by the rising of s and p valence bands relative to any d or f bands which might be present. Thus it is not entirely an accident that the $6s$-$5d$ electronic transition coincides roughly with the overlap of the Xe cores. This correlation is of course subject to the proximity of d or f bands to the Fermi level. Furthermore, the explanation[6,7] of the shock anomaly in terms of melting was contingent on an anomalous melting curve, having a region of decreasing melting temperature with increasing pressure. This occurs in the case of Cs (Ref. 13) and is believed to be due to the different rates at which the electronic transition occurs in the liquid relative to the solid.[7,13]

It is the purpose of the present paper to resolve some of the ambiguity in the understanding of the high-pressure behavior of the rare earths, by reporting a first-principles calculation of the equation of state of La, both at zero and finite temperature. La was chosen because its $4f$ band lies initially above the Fermi level, and hopefully the complexity surrounding the localized nature of $4f$ electrons in the latter rare earths is absent. Our results show that both the termination of the $6s$-$5d$ transition and the onset of significant pressure contribution from overlap of the Xe cores do occur in the vicinity of the observed stiffening in the shock data. However, the core contribution is found to be a much more gradual effect, and the abrupt nature of the anomaly evident in the data is due principally to the termination of the $6s$-$5d$ transition. Calculation of the melting temperature using a Slater model for the Grüneisen parameter, in conjunction with the band-theory pressure-volume results, does not show any region of anomalous decrease with increasing pressure. While we do estimate melting to occur along the Hugoniot in the vicinity of the shock anomaly, we are able to explain the data without including any effects of melting. Indeed, these melting effects are estimated to be small, consistent with the fact that it has not yet proved possible to detect the occurrence of melting for any metal solely from shock compression pressure-volume data.

This paper is primarily concerned with equation-of-state effects. Analyses of the La band structure below 100 kbars in regard to anomalies in the superconducting transition temperature have been reported elsewhere.[14,15] It might also be of considerable interest to correlate the calculated stiffening of the La lattice with the observed saturation of the superconducting transition temperature (at about 12 K) which takes place in the pressure region of 200 kbars.[16] The $T=0$ Grüneisen parameter calculated in the present work begins to increase with pressure in precisely this region.

In the remainder of the paper, the LMTO calculations are discussed in Sec. II, and the Grüneisen parameter and shock Hugoniot calculations are reported in Sec. III.

II. LMTO CALCULATIONS

Zero- and finite-temperature LMTO calculations of the fcc La pressure and bulk modulus are described here for the case of a static lattice of nuclei. Corrections for nuclear thermal motion are treated in the next section. In the region from 40–50% compression, the bulk modulus isotherms exhibit a rapid stiffening, which diminishes with increasing temperature. By analysis of the angular momentum decomposition of the valence charge and pressure, this anomaly can be identified with the termination of electronic $6s$-$5d$ transition, i.e., the rising of the $6s$ band above the Fermi level. A simple model calculation shows that the major effects of this electronic transition can be understood in terms of gross features of the band structure, and thus detailed analyses in the vicinity of Lifshitz singularities are not particularly useful. This seems most reasonable in view of the common occurrence of the stiffening phenomenon among the earlier transition metals.

A. Computation details

The LMTO method has been described in great detail elsewhere.[1] Its major virtue is a 2 order-of-magnitude increase in speed over more rigorous augmented-plane-wave (APW) or Korringa-Kohn-Rostocker (KKR) methods, with only small loss in accuracy. Such speed is essential for the case of La as a very dense sampling of the Brillouin zone is needed to obtain meaningful pressures in the presence of significant band crossing at the Fermi level.[10] The present calculations employed the Barth-Hedin exchange-correlation potential,[17] carried all angular momentum expansions through $l=3$, and treated all electrons self-consistently, with core states handled in a self-consistent atomic manner. The $5s$, $5p$, and higher states were treated as bands: the $5s$ and $5p$ with 20 points in the irreducible wedge of the fcc Brillouin zone, and the $6s$, $5d$, and higher states with 505 points in the irreducible wedge (for zero temperature). Relatively small Brillouin-zone sampling of inner, filled shells is known to be accurate and saves computation time.

The calculations were semirelativistic in the sense that mass-velocity and Darwin contributions were included, but spin-orbit splitting was omit-

ted, as has been discussed elsewhere.[1] When run in a nonrelativistic mode, the present program gives a zero-pressure volume for La some 40% less than that obtained for the correct relativistic case. This can be understood in terms of the increased number of repulsive s and p versus attractive d and f electrons in the relativistic case, where the mass-velocity and Darwin corrections shift the s and p bands down relative to the d and f bands. We find negligible relativistic corrections to the zero-pressure volume for neighboring Xe, consistent with the fact that the $5d$ and $4f$ bands in Xe lie well above the Fermi level at zero pressure, so that the position of the s and p bands relative to the d and f bands in this case is unimportant for the calculated pressure.

We have included both the corrections to the atomic sphere approximation (ASA) of Andersen[1] and muffin-tin correction of Glötzel and Andersen,[18] each of which amounts to about 10% in pressure for La in the vicinity of 2 Mbars. The former is included in the self-consistent loop of the band-structure calculations as described by Andersen.[1] Since the ASA corrections lead to wave-function normalization on the Wigner-Seitz polyhedron, the state l weights defined by integration over the Wigner-Seitz sphere no longer sum to unity. In this matter, we have followed the procedure of Williams *et al.*[19] and reduced the f weight, or if it would go negative, also the d weight, to achieve unity for the sum. To test this rather *ad hoc* procedure, as well as the muffin-tin correction, we developed a muffin-tin version of the program by extending the wave functions beyond the muffin-tin radius using Bessel functions of the correct energies. In this case there is no ambiguity in regard to either the normalization or the Madelung term.[18] This test program yielded pressures within 0.5% of our LMTO program with ASA and muffin-tin corrections for the case of fcc Xe over the range 0–1 Mbar. Near 1 Mbar, the ASA and muffin-tin corrections to the pressure for Xe also amount to about 10% each, and about 10% of the $5s$ and $5p$ band charge is d and f in character.

Temperature may be included in the equations in a straightforward manner.[20] Fully self-consistent calculations were done at five finite temperatures ranging from 0.05 to 0.25 Ry. Even for the lowest, the smearing effect of the Fermi-Dirac function has virtually eliminated the problem of Brillouin-zone sampling sensitivity encountered at $T=0$, so that all bands could be treated with only 20 points in the irreducible wedge. For each temperature, sums over states were carried out up to an energy cutoff $10k_BT$ above the chemical potential. The general temperature-dependent equations used to evaluate the spherically averaged charge density, total energy, pressure, and entropy in the present work are

$$\rho(r)=\frac{1}{4\pi N}\sum_{il} f_i w_{il}\left(\varphi_{il}^2(r)+\frac{\psi_{il}^2(r)}{c^2}\right), \tag{1}$$

$$E(V,T)=\frac{1}{N}\sum_i f_i\epsilon_i - 2\pi\int_0^S dr\, r^2\rho(r)\left(\frac{Ze^2}{r}+V(r)+v_{xc}(r)-2\epsilon_{xc}(r)\right), \tag{2}$$

$$P(V,T)=\frac{1}{4\pi S^2 N}\sum_{il} f_i w_{il}\varphi_{il}^2(S)\{[\epsilon_i-\epsilon_{xc}(S)]S^2+(D_{il}-l)(D_{il}+l+1)\}, \tag{3}$$

$$S(V,T)=-\frac{1}{N}k_B\sum_i [f_i\ln(f_i)+(1-f_i)\ln(1-f_i)], \tag{4}$$

where f_i is the Fermi-Dirac function

$$f_i=\{\exp[\beta(\epsilon_i-\mu)]+1\}^{-1}, \tag{5}$$

μ is the chemical potential, and S is the Wigner-Seitz radius. The one-electron energies are ϵ_i, the corresponding normalized large and small component radial wavefunctions are $\varphi_{il}(r)$ and $\psi_{il}(r)$, the state l weights are w_{il}, and logarithmic derivatives $D_{il}=D_l(\epsilon_i)=S\varphi_{il}'(S)/\varphi_{il}(S)$. Normalization of the radial wave functions is $\int_0^S dr\, r^2 \times[\varphi_{il}^2(r)+\psi_{il}^2(r)/c^2]=1$. The total one-electron potential is $V(r)$, the exchange-correlation potential is $v_{xc}(r)$, and the corresponding energy density is $\epsilon_{xc}(r)$. For convenience the index i combines $\vec{k}$ vector and band index, and runs over the full Brillouin zone so that symmetry weighting need not be shown. The muffin-tin corrections[18] added to the energy and pressure are

$$\Delta E=\alpha q^2/S, \tag{6}$$

$$\Delta P=-\frac{\partial(\Delta E)}{\partial V}\bigg|_T, \tag{7}$$

where $\alpha=0.008\,25$ Ry bohr for the fcc lattice, and $q=4\pi S^3\rho(S)/3$. Equation (3) is just the Pettifor-Liberman surface integral,[21] appropriate in this nonrelativistic form as $V(S)/c^2\ll 1$ at the Wigner-Seitz radius. Equation (2) is formally correct in either non- or fully-relativistic limits, but represent a perturbation treatment in the present semirelativistic case. Nevertheless, we find by numerical integration of the pressure that the virial theorem is satisfied in the present work both at $T=0$ and at finite temperatures to within the convergence uncertainties in $E-ST$.

B. Zero-temperature calculations

Theoretical results for the $T=0$, fcc La pressure and bulk modulus are shown in Figs. 1 and 2, respectively. Each quantity is resolved into valence, core, and muffin-tin correction contributions. In Fig. 2, the solid line is a fit to the data points obtained by direct numerical differentiation of calculated pressures.[22] The scatter, which mainly originates from the valence contribution, is characteristic of Brillouin-zone sampling sensitivity,[23] and indicates that substantially more than 505 points per irreducible wedge would be needed to obtain entirely smooth pressure derivatives at $T=0$. Nevertheless, these results are entirely adequate for the purposes of this work. Both figures show the room-temperature measurements of Syassen and Holzapfel[24] (dotted curves). Since room-temperature thermal corrections amount to only a few kbars in pressure, it can be seen (Table I) that the calculated zero-pressure volume is too small by 7%, and the calculated normal density bulk modulus is too small by 12%. The principal numerical difference between these results and those of Glötzel,[14] which extend up to only about 100 kbars, is our inclusion of the muffin-tin correction, as ASA corrections to the pressure are negligible for La in this range.

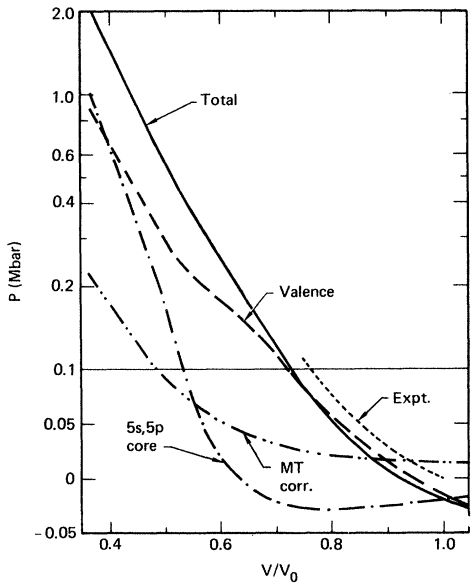

FIG. 1. $T=0$ pressure versus relative volume for fcc La. The calculated total pressure (solid curve) is shown resolved into valence, 5s and 5p core, and muffin-tin correction contributions (dashed curves). Experimental results of Syassen and Holzapfel (Ref. 24) are shown as the dotted curve. Note scale change at 0.1 Mbar.

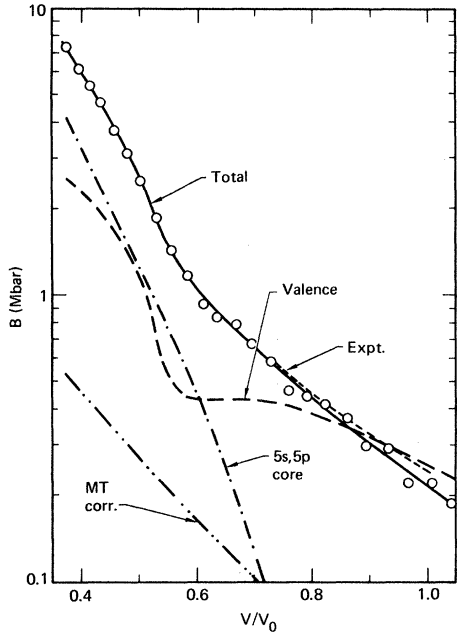

FIG. 2. $T=0$ bulk modulus versus relative volume for fcc La. The total calculated bulk modulus (numerical differentiation, data points; smoothed fit, solid curve) is resolved into valence, 5s and 5p core, and muffin-tin correction contributions (dashed curves). The experimental results of Syassen and Holzapfel (Ref. 24) are shown as the dotted curve.

The existence of an anomaly is most evident in Fig. 2. The bulk modulus undergoes rapid stiffening between $V/V_0=0.57-0.5$ ($V_0=251.7383$ bohr^3). While the 5s and 5p core contribution is certainly becoming important in this range, it is the more dramatic stiffening seen in the valence contribution which is primarily responsible for the anomaly. This structure comes from the s

TABLE I. Calculated and experimental Wigner-Seitz radius and bulk modulus for fcc La at zero pressure and temperature.

	Wigner-Seitz radius (bohr)	Bulk modulus (kbar)
Calculated		
Glötzel (Ref. 14)	3.77	240[a]
Present	3.82	218[a]
		280[b]
Experiment[c]		
Syassen and Holzapfel (Ref. 24)	3.917	248

[a] At experimental zero pressure and volume.
[b] At calculated zero pressure and volume.
[c] Room temperature.

component of the bulk modulus as is evident in Fig. 3, where both the valence pressure and bulk modulus are resolved into angular momentum components, P_l and B_l. The anomaly can furthermore be correlated with the variation of the s occupation number $n_s = \sum f_i w_{is}$ shown in Fig. 4. The rapid increase in $B_s = -dP_s/d\ln V$ for $V/V_0 = 0.57 - 0.5$ coincides with the same behavior in $-dn_s/d\ln V$.

To understand the relation between P_s (or B_s) and n_s in detail, we turn to canonical band theory. Within the atomic-sphere approximation one may write the pressure relation Eq. (3) in the following form[25]:

$$3PV = -\delta\left(\int^{\epsilon_F} d\epsilon\, \epsilon N(\epsilon)\right)\Big/\delta \ln S \tag{8}$$

which essentially is the variation in the sum of one-electron energies. $N(\epsilon)$ is the state density and S is the Wigner-Seitz radius ($\frac{4}{3}\pi S^3 = V$). For our purpose Eq. (8) may be decomposed into angular momentum components, and to first order in energy we obtain for the s partial pressure[25]

$$3P_sV = -n_s\left(\frac{\delta c_s}{\delta \ln S} + (\bar{E}_s - c_s)\frac{\delta \ln W_s}{\delta \ln S}\right) \tag{9}$$

$$\equiv n_s\left(-\frac{\delta \epsilon}{\delta \ln S}\right)_s \tag{10}$$

where c_s, $\bar{E}_s$, and W_s are the center, the center of gravity, and the width of the 6s band. Equation (9) may easily be evaluated, and it provides a good estimate of the s pressure for $V/V_0 > 0.5$ as seen in Fig. 5. Below this volume the s charge arises from the tails of occupied d and f orbitals, and so expansion about the center of the 6s band becomes inaccurate. The variation of the s pressure may be understood if we note that $3P_sV$ is a product of two terms: one, $-\delta\epsilon/\delta \ln S$, which

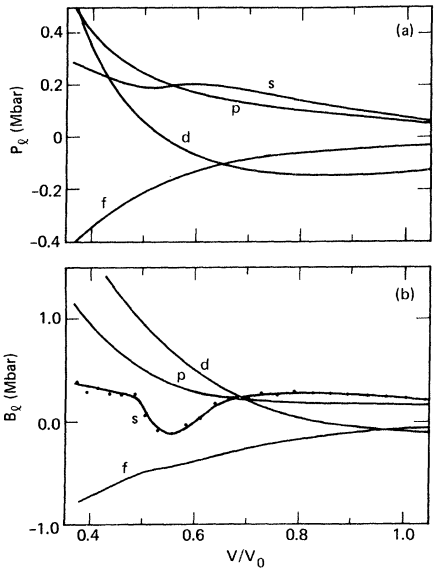

FIG. 3. $T = 0$ valence pressure and bulk modulus, resolved into angular momentum components, versus relative volume. (a) Pressure, P_l. (b) Bulk modulus, $B_l = -dP_l/d\ln V$. Data points show the direct results of numerical differentiation used to obtain B_s.

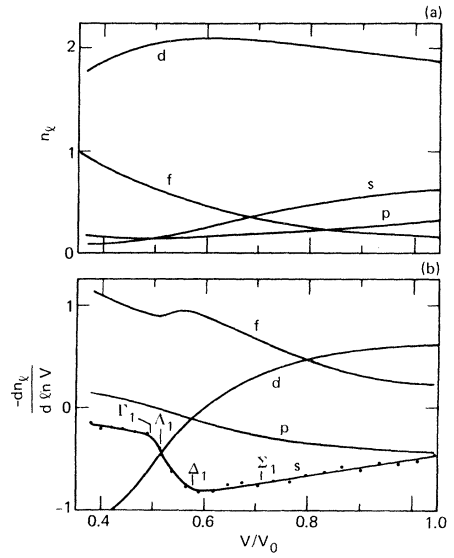

FIG. 4. $T = 0$ number of valence electrons and logarithmic volume derivatives, resolved into angular momentum components, versus relative volume. (a) Number of l electrons, n_l. (b) Logarithmic volume derivative, $-dn_l/d\ln V$. The locations of Lifshitz singularities relevant to the s band are marked. Data points show the direct results of numerical differentiation used to obtain $-dn_s/d\ln V$.

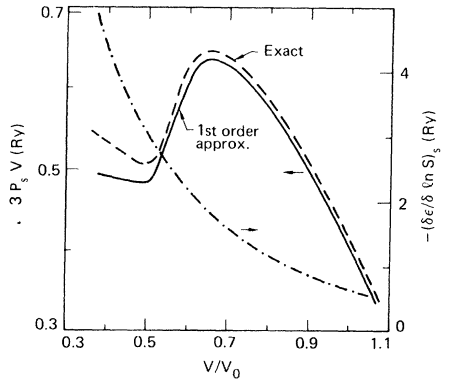

FIG. 5. Canonical band analysis of the s-valence pressure. Exact results for $3P_sV$ (dashed curve), first-order approximation to $3P_sV$ based on Eq. (10) (solid curve), and average change in the one-electron energy per electron as defined in Eq. (10), $-(\delta\epsilon/\delta \ln S)_s$ (dash-dot curve) versus relative volume.

describes the average change in one-electron energy per electron and which has a smooth volume variation, Fig. 5, and the other, n_s, which depends on the finer details of the band structure. At first $-\delta\epsilon/\delta\ln S$ changes faster than n_s, and P_s increases almost linearly so that the s bulk modulus is almost constant over a large volume range. Then at $0.64V_0$ the s occupation (Fig. 4) changes faster than $-\delta\epsilon/\delta\ln S$ and a maximum in P_s is developed (Figs. 3 and 5) and B_s goes through zero. Eventually, when n_s levels out, $-\delta\epsilon/\delta\ln S$ takes over once more, and the pressure and the bulk modulus rise again.

The volume dependence of the valence n_l shown in Fig. 4 can be understood by considering the unhybridized l-band edges shown in Fig. 6, divided by the correct Fermi energy ϵ_F to emphasize band crossing at the Fermi level. Note first the broadening of the 5s and 5p core bands. The valence bands are 6s, 6p, 5d, and 4f. The 6p and over most of the range also the 4f bands are empty, so that the number of p and f valence electrons n_l seen in Fig. 4 arises from hybridization. The upward motion of the 6s band through the 5d band (Fig. 6) leads to an s-d electronic transition which terminates at $V/V_0=0.5$, as the bottom of the 6s band Γ_1 rises above the Fermi level. Figure 4(b) shows that the transition is, in fact, primarily s to f for $V/V_0<0.8$. This follows from the increasing f character of the 5d states below ϵ_F brought about by their hybridization with the 4f band, which is moving slowly downward relative to the Fermi energy (see Fig. 6). We shall still conveniently refer to this transition as s-d in reference to the principal *bands* involved, the 6s and 5d. As indicated by the

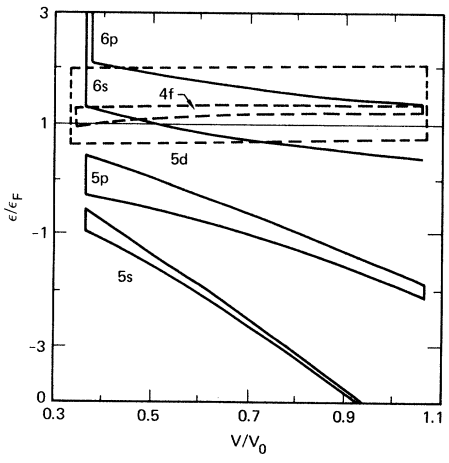

FIG. 6. $T=0$ unhybridized l-band edges versus relative volume. Energies are divided by the correct Fermi energy to emphasize band crossing at the Fermi level, $\epsilon/\epsilon_F=1$.

arrow in Fig. 4(b), the end of the s-d transition at $V/V_0=0.5$ coincides with the end of the abrupt increase in $-dn_s/d\ln V$ which began near $V/V_0=0.57$. The quantity $dn_s/d\ln V$ is simply the rate at which s electrons are converted to df hybrids in the course of compression. One may view [Eq. (10)] the negative slope of the levels in Fig. 6 as an effective pressure per electron. Since s levels move up relative to d or f levels, conversion of a 6s electron to 5d or 4f states thus serves to reduce the pressure and bulk modulus. This softening effect should be largest near $V/V_0=0.57$, where 6s electrons are lost at the greatest rate, and should terminate by $V/V_0=0.5$ when all 6s electrons have been converted.

The significance of $V/V_0=0.57$ as the beginning of the end of the s-d transition may be found by examination of the band structure, shown in Figs. 7 and 8 for $V/V_0=0.99$ and 0.57, respectively. The dominant 6s character occurs around Γ_1, 4f around $\Gamma_{2'}$, and the 5d around X_1 and X_3. Moving out from Γ_1, the state s weights drop to $\frac{1}{2}$, very close to the maxima in the Λ_1, Δ_1, and Σ_1 branches (except at the largest V/V_0), beyond which the states become predominantly 5d in character. This suggests a simple model, illustrated schematically in Fig. 9, according to which the relevant pocket of 6s states lies within a $\vec{k}$-space surface whose radius in symmetry directions is given by the dotted lines in the figure. At first, the s-d transition proceeds entirely by the continuous conversion of 6s to 5d states via hybridization, and the pocket shrinks in size. Then at $V/V_0=0.72$ the Σ_1 maximum passes above the Fermi level, and the previously fully occupied 6s pocket begins to be emptied, accelerating the rate of s-d transition. The maximum density of 6s states occurs at $\epsilon(\vec{k})$ where $\vec{k}$ lies between the outermost bump and the innermost dimple of the pocket surface. In the important range of V/V_0, this occurs at the Δ_1 maximum. Thus as the Δ_1 maximum passes above ϵ_F at $V/V_0=0.57$, the s-d transition has achieved its greatest rate, and then rapidly exhausts itself until at $V/V_0=0.50$ the Γ_1 state passes above ϵ_F and the transition is over.

We suggest that the model defined in Fig. 9 exhibits the essential physics of the s-d transition in La. This may be verified by comparing the model prediction for the important quantity $-dn_s/d\ln V$ to Fig. 4(b). Accordingly, the $\vec{k}$-space volumes indicated in Fig. 9 were numerically evaluated to obtain the number of 6s electrons, and then differentiated to get $-dn/d\ln V$ shown in Fig. 10. The agreement with $-dn_s/d\ln V$ in Fig. 4(b) is indeed quite good throughout the region where the s-d transition is in progress, i.e.,

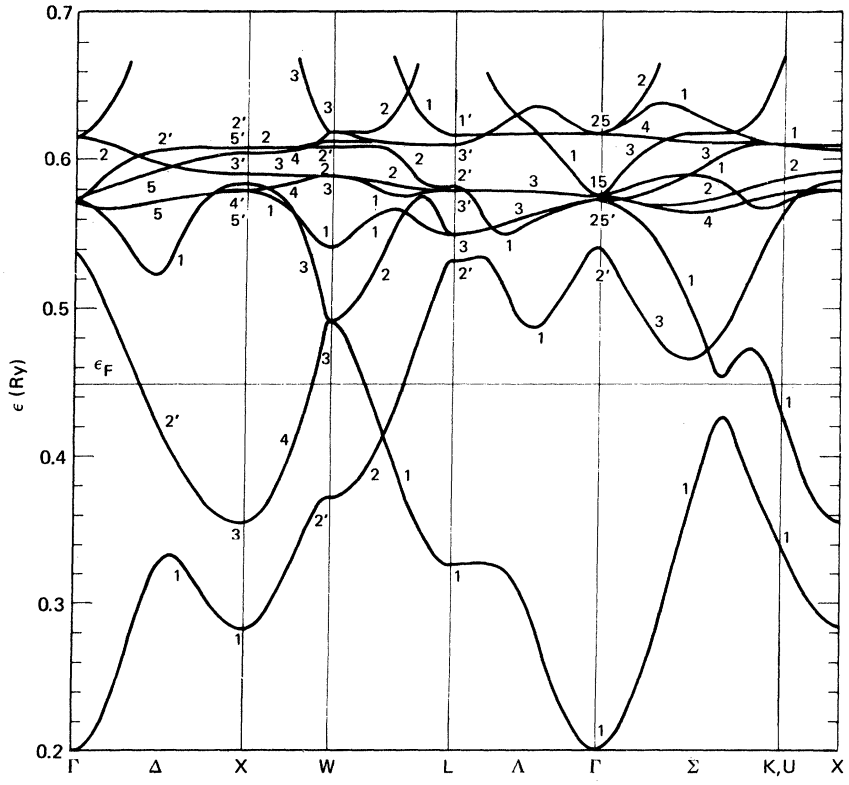

FIG. 7. Band structure for $T=0$ fcc La at $V/V_0=0.99$. The Fermi energy is ϵ_F. All energies are relative to the value of the one-electron potential at the Wigner-Seitz radius.

$V/V_0>0.5$.

Lifshitz singularities[26] will occur during the s-d transition as extrema of the various branches pass through the Fermi energy, leading to local analytic changes in $dn_s/d\ln V$ as can be seen in Fig. 10. These local analytic changes are overshadowed by the scatter in Fig. 4(b). They are, in fact, exaggerated in Fig. 10, as the model treats states at the branch maxima as totally s in character. The important point, however, is that the analytic changes are small, and according to Eq. (10), should lead to only minor structure in the bulk modulus. Thus the major effects of the s-d transition in La are reproduced in our calculations in Figs. 2 and 3, and follow from the rough, overall shape of $dn_s/d\ln V$. With this in mind, it seems unlikely that low-order expansions,[26,27] valid only near individual Lifshitz singularities, will offer full insight into the nature of the s-d transition in La. Not only does the overall shape of the curve in Fig. 10 involve a confluence of four Lifshitz singularities, but there are important non-Fermi-surface effects for $V/V_0>0.72$. In this range, the s-d transition proceeds by the shrinking of the 6s electron pocket, the result of hybridization between the 6s and 5d bands. Such behavior also occurs for Cs below the 42.5-kbar isostructural transition, and is known to have a softening effect.[8,10]

C. Finite-temperature calculations

Results for the isothermal bulk modulus of La are shown in Fig. 11 for six temperatures ranging from 0 to 0.25 Ry (3.4 eV) in increments of 0.05 Ry. The pressure and total energy were evaluated by fully self-consistent finite-temperature LMTO calculations at 24 volumes for each isotherm. The thermal electron pressure, $\Delta P_e=P(V,T)-P(V,0)$, ranges from 0.28 to 0.79 Mbar at the highest temperature for $V/V_0=1-0.4$. Scatter in numerical derivatives of the finite-temperature pressures was negligible, so that only an analytic fit to our calculated $\ln(B)$ is shown in the figure. The overall rms deviation from the fit of some 140 numerical derivative values of $\ln(B)$ is 0.02% or 0.6% of the range of variation of this quantity seen in the figure.

Note that the two lowest $\ln(B)$ isotherms in Fig. 11 cross at $V/V_0=0.53$ and perhaps again near $V/V_0=0.75$. This is by no means in violation of thermodynamics, as can be seen from the usual low temperature electronic expansions,

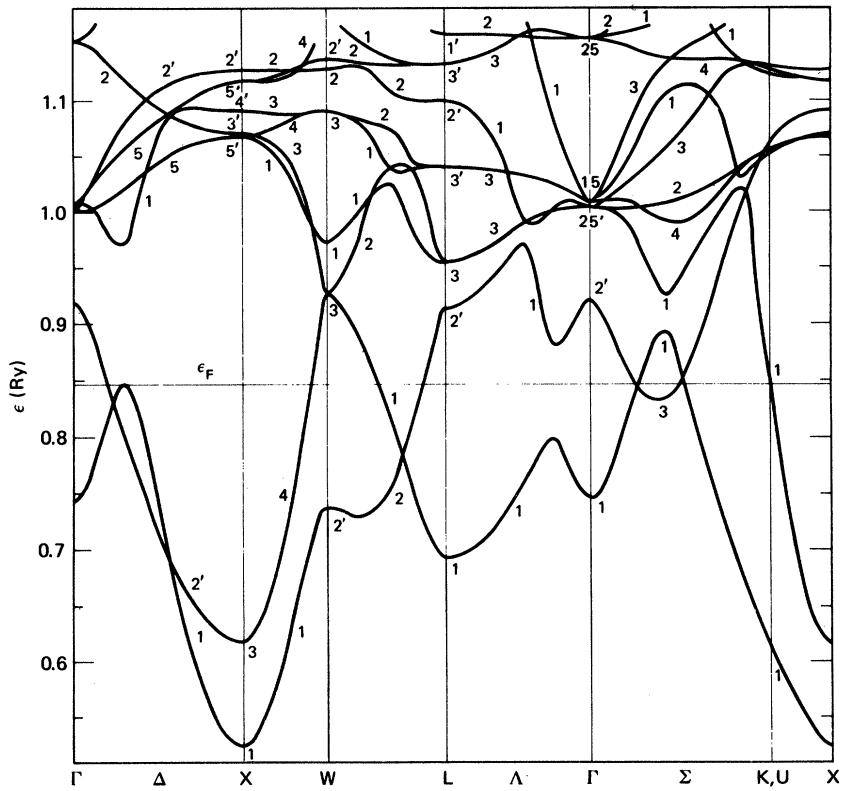

FIG. 8. Band structure for $T=0$ fcc La at $V/V_0=0.57$. The Fermi energy is ϵ_F. All energies are relative to the value of the one-electron potential at the Wigner-Seitz radius.

$$\Delta E = gT^2/2\,,$$

$$\Delta P = g'T^2/2\,,$$

$$\Delta(\ln B) = -(Vg''/2B_0)T^2\,,$$

where $g=\pi^2 k_B^2 N(\epsilon_F)/3$, $N(\epsilon_F)$ is the density of states at the Fermi level, the primes signify volume derivatives, and B_0 is the $T=0$ bulk modulus. We find that $gT^2/2$ agrees with the calculated ΔE ($T=0.05$) to within 10–30% for $V/V_0=0.35$–1. Thus $T=0.05$ Ry is not too far beyond the range of these low-T expansions, consistent with the fact that 0.05 Ry is only 10–20% of the width of the occupied part of the valence band for $V/V_0=0.35$–1. $N(\epsilon_F)$ is roughly linear in volume, with slight modulations. These modulations lead to slightly positive values of g'' in the vicinity of $V/V_0=0.5$ and near 0.75, in qualitative agreement with the behavior seen in Fig. 11.

The most important observation to be drawn from Fig. 11 is that the rapid stiffening in the bulk modulus between $V/V_0=0.57$–0.5 has been removed by the effect of temperature. This is even more evident by examining Fig. 12, the counterpart of ($T=0$) Fig. 2 at $T=0.25$ Ry. Comparision of the two figures shows that while there is some temperature dependence to the core contribution, it is primarily the smoothing of the valence contribution to the bulk modulus which has eliminated the rapid stiffening. There is of course some stiffening in the total bulk modulus which does arise from the growing 5s and 5p core contribution, as volume is decreased. However, this behavior is too gradual to be considered really unusual, as will be seen in the next section by examination of the lattice Grüneisen parameter. *Thus the electronic s-d transition, and not core overlap, is the principal cause of the anomaly at $T=0$.* The annealing effect of temperature is precisely what is expected from electronic transition anomalies. If the Fermi level is considered to have a width of, say, $2k_BT$, consideration of the volume dependence of $\epsilon(\Gamma_1)-\epsilon_F$ and $\epsilon(\Delta_1)-\epsilon_F$ shows that $T=0$ structure lying between $V/V_0=0.50$ and 0.57 will be smeared out over a range extending from $V/V_0=0.4$ to well beyond $V/V_0=1$.

III. HUGONIOT CALCULATIONS

Experimental detection of the bulk modulus anomaly described in the preceding section by

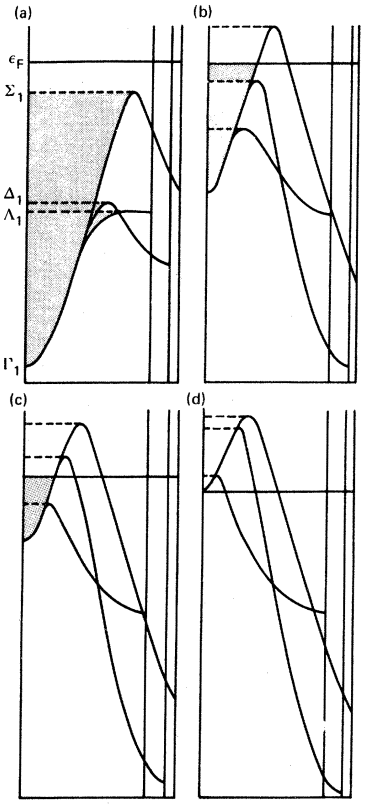

FIG. 9. Simple model for the s-d transition in La. The Λ_1, Δ_1, and Σ_1 branches are shown superposed at four volumes. (a) $V/V_0=0.99$, (b) $V/V_0=0.60$, (c) $V/V_0=0.55$, and (d) $V/V_0=0.50$. The 6s states are considered to lie inside maxima of these branches, in a nonspherical pocket in $\vec{k}$ space whose radius in symmetry directions is given by the length of the dotted lines. The shaded area below the Fermi energy ϵ_F, indicates occupied 6s states.

means of room-temperature and static compression techniques would be difficult, requiring careful analysis of the measured PV data. In contrast, the high temperatures induced by shock compression lead to a greatly increased contri-

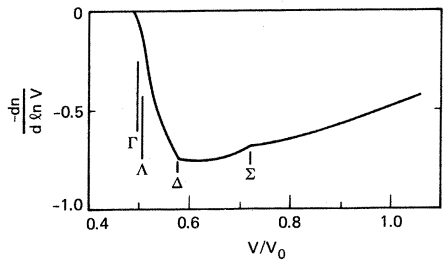

FIG. 10. Logarithmic volume derivative, $-dn/d\ln V$, of the number of 6s electrons, n, versus relative volume, according to the model in Fig. 9. The locations of Lifshitz singularities are marked.

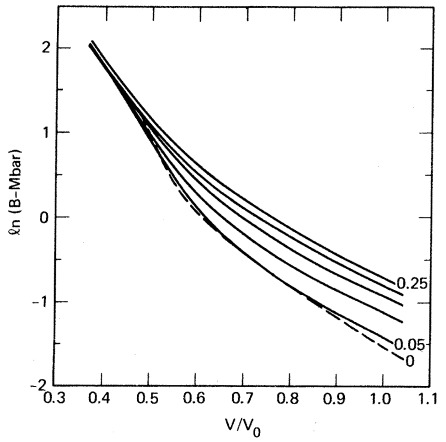

FIG. 11. Finite-temperature bulk modulus versus relative volume for fcc La. Natural logarithm of the bulk modulus in Mbar is plotted for six temperatures in increments of 0.05 Ry from $T=0$ to 0.25 Ry. No correction for nuclear thermal motion has been added.

bution to the pressure from thermal motion of the nuclei, making this technique an ideal probe of the anomaly for the following reason: The thermal nuclear motion contribution to the pressure depends, at least within the Slater[2] or similar models, on the derivative of the bulk modulus shown in Fig. 11, through the lattice Grüneisen parameter. Thus the stiffening seen in that figure leads to a large bump in the Grüneisen parameter,

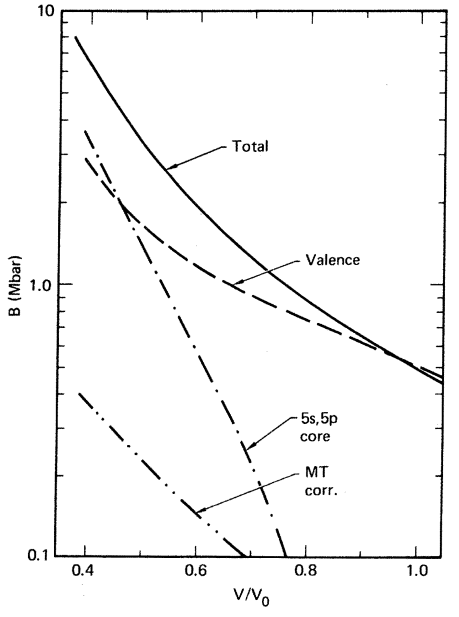

FIG. 12. $T=0.25$ Ry bulk modulus versus relative volume for fcc La. The total bulk modulus (solid curve) is shown resolved into valence, 5s and 5p core, and muffin-tin correction contributions (dashed curves). No correction for nuclear thermal motion has been added.

which results in a rapid stiffening of the shock compression curve for $V/V_0 < 0.64$, in agreement with the experimental data. We therefore identify the shock compression anomaly in La, and in the rare earths in general, with termination of the $6s$ to $5d$ electronic transition.

In a shock compression experiment, there are two fundamental experimental parameters: The shock velocity u_s is the speed with which the shock wave traverses the sample. In its passage, the shock wave imparts a net velocity to the material behind the shock front, known as the particle velocity u_p. When this process is analyzed in terms of the conservation laws of mass, momentum, and energy, the thermodynamic properties of the initial state (P_0, V_0, E_0) are related to those of the compressed state (P, V, E) by the Rankine-Hugoniot conditions (ρ_0 is the initial density):

$$P(V,T) - P_0 = \rho_0 u_s u_p , \tag{11}$$

$$V = V_0(1 - u_p/u_s) , \tag{12}$$

$$E(V,T) - E_0 = \tfrac{1}{2}[P(V,T) + P_0](V_0 - V) . \tag{13}$$

Shock compression, or Hugoniot data are presented both in a u_s vs u_p format, or by using the first two equations as P vs V. A theoretical calculation requires a complete equation of state, $E(V,T)$ and $P(V,T)$. The condition represented by Eq. (13) may then be used to solve, at each V, for the Hugoniot temperature $T_H(V)$, and thence the pressure $P = P(V, T_H)$ and u_s and u_p.

A. Equation of state

To complete the equation of state, the total energies and pressures calculated in Sec. II must be corrected for thermal motion of the nuclei:

$$E(V,T) = E_{\mathrm{SL}}(V,T) + \Delta E_n(V,T) , \tag{14}$$

$$P(V,T) = P_{\mathrm{SL}}(V,T) + \Delta P_n(V,T) . \tag{15}$$

E_{SL} and P_{SL} are the results of the finite-temperature LMTO calculations of Sec. II, i.e., Eqs. (2) and (3) plus the muffin-tin corrections Eqs. (6) and (7). We use the subscript SL as a reminder that these calculations were carried out for a static lattice of nuclei, and thus while including thermal electronic excitation, do not allow for any affect on the band structure due to the thermal nuclear motion. However, we do incorporate some aspects of the electron-phonon coupling in the nuclear thermal contributions ΔE_n and ΔP_n.

In the quasiharmonic[28] model, the free energy of a solid due to thermal motion of the nuclei is

$$\Delta F_n(V,T) = \frac{1}{N}\sum_{\vec{k}\lambda} \{\tfrac{1}{2}\hbar\omega_{\vec{k}\lambda} + k_B T \ln[1 - \exp(-\beta\hbar\omega_{\vec{k}\lambda})]\} , \tag{16}$$

where $\omega_{\vec{k}\lambda}$ are the phonon frequencies, defined in terms of second derivatives of the interaction potential for the nuclei V_n. The problem of obtaining this potential, or the frequencies themselves, for a nonsimple metal like La is exceedingly difficult, and beyond the scope of the present work. However, if we make the Debye approximation, and take the high-temperature limit, one obtains from Eq. (16)

$$\Delta E_n(V,T) = 3k_B T[1 + \delta(V,T)] , \tag{17}$$

$$\Delta P_n(V,T) = 3k_B T\gamma(V,T)/V , \tag{18}$$

where $\delta(V,T) = (\partial \ln\omega_D/\partial \ln\beta)_V$, and the nuclear or lattice Grüneisen parameter, $\gamma(V,T) = -(\partial \ln\omega_D/\partial \ln V)_T$, with $\omega_D(V,T)$ being the Debye frequency. We take the Debye frequency to be temperature dependent since the interaction potential V_n for the nuclei must depend on the temperature of the thermally excited electron system. Indeed, a finite-temperature generalization of the Born-Oppenheimer approximation[29] indicates that V_n is just the free energy of the static lattice system treated in Sec. II for the equilibrium arrangement of the nuclei. Furthermore, it can be argued[29] that the electrons may be treated isothermally for lattice distortions corresponding to the short-wavelength phonon excitations which dominate the equation of state, so that

$$\omega_D^2(V,T) = c^2 k_D^2 \sim B_{T,\mathrm{SL}} V^{1/3}$$

where $B_{T,\mathrm{SL}}$ is just the isothermal bulk modulus for the static lattice system, i.e., the quantity plotted in Fig. 11. Using this relation, $\delta(V,T)$ and the lattice Grüneisen parameter $\gamma(V,T)$ may be written

$$\delta(V,T) = \tfrac{1}{2}\left(\frac{\partial \ln B_{T,\mathrm{SL}}(V,T)}{\partial \ln\beta}\right)_V , \tag{19}$$

$$\gamma(V,T) = -\frac{1}{6} - \frac{1}{2}\left(\frac{\partial \ln B_{T,\mathrm{SL}}(V,T)}{\partial \ln V}\right)_T . \tag{20}$$

The lattice Grüneisen parameter is generally expected to be temperature independent and smoothly decreasing with compression.[30] Evaluation of Eq. (20) for the present case of La, however, shows (Fig. 13) a dramatic and temperature-dependent peak in this parameter. Note that an exponential dependence of the bulk modulus leads to a linear γ according to Eq. (20). Furthermore, a sum of exponentials, chosen to approximate the $5s$ and $5p$ core plus the p- through f-valence contributions to the bulk modulus (Figs. 2 and 3), yields only rather small modulations in γ. Thus it is indeed the s component of the valence bulk modulus which has caused the truly anomalous stiffening in the static lattice bulk modulus, responsible for the large peak seen in Fig. 13.

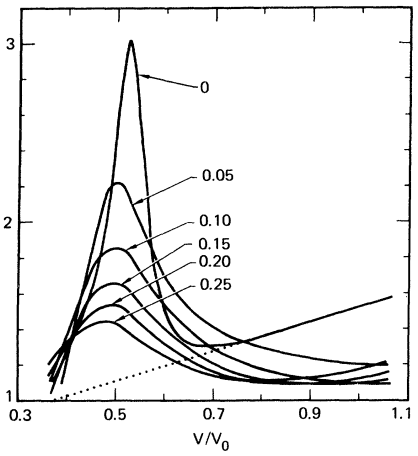

FIG. 13. Finite-temperature lattice Grüneisen parameter, $\gamma(V,T)$, versus relative volume for fcc La. The Slater model results (solid curves) are shown for six temperatures in increments of 0.05 Ry ranging from $T=0$ to 0.25 Ry. The dotted line is a temperature independent linear $\gamma(V)$ used for a comparison calculation.

As discussed earlier, this is due to termination of the electronic s-d transition. As the softening effect of the electronic transition begins to run out, the phonon frequencies undergo a region of rapid increase with compression, leading to the peak in $\gamma=-(\partial\ln\omega_D/\partial\ln V)_T$. As temperature is increased, and the electronic transition is washed out, the size of this peak is rapidly reduced. This temperature dependence is a direct manifestation of electron-phonon coupling, which is thus partially included in these calculations as alluded to earlier.

Equation (20) is the usual Slater[2] model for the Grüneisen parameter, generalized to finite temperatures. The closely related Dugdale-MacDonald and free-volume models[30] yield slightly higher peaks in γ, but smaller (or negative) slopes for $V/V_0>0.7$, leading to $V/V_0=1$ values decreased by the amounts 0.33 and 0.67, respectively. Combined with an uncertainty of about ±0.2 due to the choice of the analytic fit to $B_{T,\mathrm{SL}}$, the free-volume model would then be in best agreement with the thermodynamic value of 0.74 for γ of dhcp La at room temperature and $V/V_0=1$.[31] (Room-temperature La is dhcp below about 23 kbars, but can be maintained in metastable fcc form down to atmospheric pressure.[32]) Since the Hugoniot is insensitive to the value of γ for $V/V_0>0.7$, we have used the Slater model because of its simpler interpretation of γ as essentially the slope of the bulk modulus.

None of the various γ models shows any tendency to yield negative values of γ for La, due to s-d transition softening, in contrast to similar calculations for Cs, where a region of negative γ appears to explain the observed isostructural transition at room temperature.[9] This difference may be understood from Eq. (10). However, for simplicity, we will not decompose states into angular momentum components, but rather divide them in the spirit of Fig. 9 into upward moving 6s and downward moving 5d categories. On summing over states and differentiating, one then has

$$3BV\sim 3B_0V+\left[\left(\frac{\delta\epsilon}{\delta\ln S}\right)_{6s}-\left(\frac{\delta\epsilon}{\delta\ln S}\right)_{5d}\right]\left(\frac{dn_{6s}}{d\ln V}\right),$$

where B_0 (positive) is the bulk modulus in the absence of electronic transition ($\Delta n_{6s}=0$), and the second term (negative) is the softening effect due to the s-d transition. It is the balance between these two terms which determines the *relative* importance of the softening effect on the total bulk modulus and on γ. With this in mind, one may identify two specific differences between La and Cs; the first, quantitative; the second, qualitative. First, only about one of the three valence electrons is involved in the s-d transition for La (there are already two d electrons at $P=0$), while all (the single 6s) valence electrons are involved for Cs. Since all valence electrons contribute to B_0, this term is relatively more important for La than Cs. Second, hybridization between the 6s and 5d bands tends to decrease the rate at which 6s electrons are lost, $-dn_{6s}/d\ln V$, in comparison to the rate which would occur in the absence of hybridization. In Cs the negative region in γ occurs when a pocket of pure d states (near X_3) passes below ϵ_F, so that $-dn_{6s}/d\ln V$ is especially large. This effect is absent for La, since the X_3 pocket is already below ϵ_F at $P=0$.

B. Hugoniot results

Hugoniot calculations were carried out entirely for an fcc phase of La. As noted, La is dhcp below about 23 kbars and the high temperatures induced by shock compression cause the fcc solid to melt above about 360 kbars (see below) along the Hugoniot. However, the difference in equation of state between the two close packed solid phases should be slight, and we argue subsequently that also the liquid corrections at the pressures considered here are small. Equation (13) was solved taking room-temperature and $V=V_0$ initial conditions, and the equation-of-state model defined by Eqs. (14), (15), and (17)–(20). A small constant pressure shift of 14 kbars and corresponding energy shift was made to the results of the preceding section to bring the room-temperature, one-atmosphere volume into agreement with experiment.

The calculated u_s-u_p results (solid curve) are compared in Fig. 14 to the experimental data. The fit of Ref. 6 (two dashed lines) is shown for comparison. Hugoniot data for many materials can be fit by a linear u_s-u_p relation, with a change in slope indicating a phase transition. It is for this reason that La has been assumed to undergo a phase transition at $u_p = 1.04$ km/sec, or $V/V_0 = 0.64$, where the two dashed lines cross. However, it should be noticed that the upper dashed line does not account for all of the high-pressure data. Furthermore, recent theoretical calculations for a variety of materials have cast doubt on the linear u_s-u_p rule of thumb. The present results for La (solid curve) in fact vary smoothly over the entire range of the figure. The curve is approximately linear at small u_p, with a $u_p = 0$ intercept too small by 7%. This intercept is the bulk sound speed and is off because the $V/V_0 = 1$ bulk modulus in Fig. 2 is too small by 12%. Self-consistent band theory generally gives the normal density bulk modulus to within about 20% of experiment, so this offset is not unexpected. The important feature of these calculations is the upward turn of the u_s-u_p curve for $u_p > 1$ km/sec, and the gradual bending over at the highest values of u_p. This is due to the bump in γ. To show this, the calculations were repeated for a linear, temperature-independent γ without the bump (dotted curve, Fig. 13). The corresponding Hugoniot curve is the dotted curve in Fig. 14. The solid curve is seen to bow upward and then bend back towards the dotted curve as γ approaches and then passes its maximum.

A PV plot of the Hugoniot data is shown in Fig. 15. The calculated Hugoniot pressure is resolved into zero-temperature, electron thermal $\Delta P_e(V,T) = E_{SL}(V,T) - E_{SL}(V,0)$, and nuclear thermal parts for comparison. As before, the dotted curve shows the Hugoniot for the linear γ. The upward bend of the solid curve for $V/V_0 < 0.64$ is seen to arise from the rapid increase of the nuclear thermal contribution, which in turn comes from the rapid increase in γ. The Grüneisen parameter along the Hugoniot, $\gamma(V, T_H)$ is shown in Fig. 16. The effect from the nuclear thermal contribution is largest at $V/V_0 = 0.54$ where $\gamma(V, T_H)$ is maximum, and then runs out as $\gamma(V, T_H)$ decreases for smaller volumes. The calculated solid curve in Fig. 15 lies above the data by about 14% at $V/V_0 = 0.54$, resulting from the maximum in $\gamma(V, T_H)$ which is apparently too large by 13%. This is not too surprising given the crudeness of

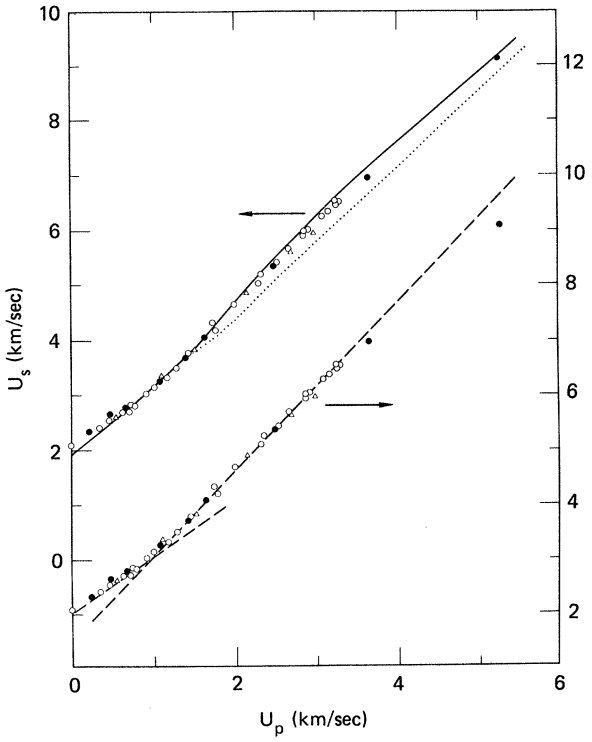

FIG. 14. Theoretical and experimental results for the La Hugoniot; shock velocity u_s versus particle velocity u_p. Present calculation with temperature-dependent Slater γ (solid curve) and temperature-independent linear γ (dotted curve). The two-line fit of Ref. 6 (dahsed lines) is shown for comparison. The data are from Ref. 3 (●), Ref. 5 (△), and Ref. 6 (○).

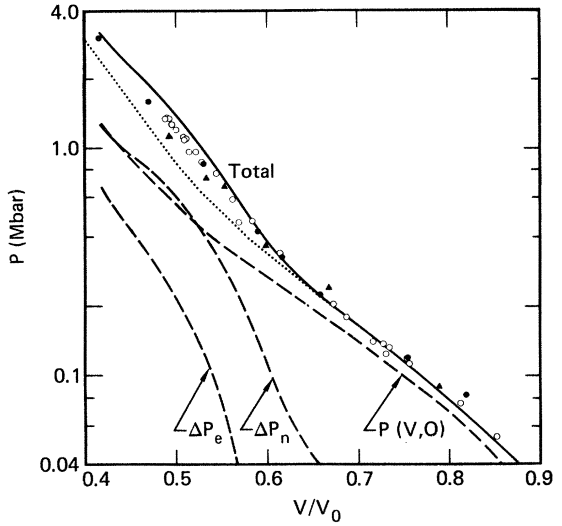

FIG. 15. Theoretical and experimental results for the La Hugoniot; pressure versus relative volume. Present calculation with temperature-dependent Slater γ (solid curve) and with temperature-independent linear γ (dotted curve). The total pressure (solid curve) is shown resolved into zero temperature, $P(V,O)$; electron thermal, ΔP_e; and nuclear motion thermal, ΔP_n contributions (dashed curves). The data is from Ref. 3 (●), Ref. 5 (▲), and Ref. 6 (○).

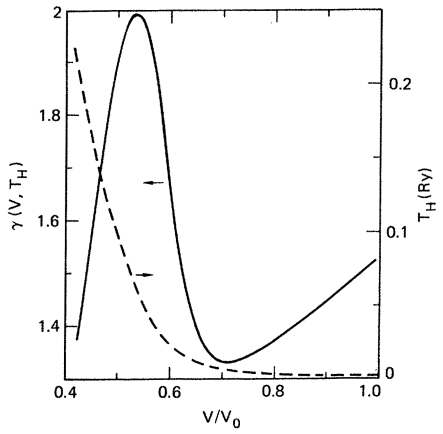

FIG. 16. Slater-model Grüneisen parameter (solid curve) and temperature (dashed curve) along the Hugoniot versus relative volume.

the Slater model. Nevertheless, we believe the almost quantitative agreement in Fig. 15 bears out our contention that the essential anomaly in the La shock data follows from a peak in the lattice Grüneisen parameter, which in turn is due to the termination of the electronic s-d transition.

The temperature dependence of $\gamma(V,T)$ is crucial to the present work. A temperature-independent $\gamma(V)$ equal to $\gamma(V,0)$ in Fig. 13 yields unphysical double valued results for the function $u_s(u_p)$; the rapid drop to the low-volume side of the peak in $\gamma(V,0)$ causing u_p to momentarily decrease with compression. This is not because the $T=0$ peak is excessively high through any attempt of our $\ln(B)$ fit to model divergences in $\partial B/\partial V$ which should occur at Lifshitz singularities. We have argued earlier that the behavior of $B_{T,\mathrm{SL}}(V,0)$ leading to the peak in $\gamma(V,0)$ is governed by more coarse features of the electron density of states, and thus any Lifshitz singularities in the Slater model $\gamma(V,0)$ will be more in the nature of decorations on the structure in Fig. 13, of short range in V/V_0. The important point in regard to the Hugoniot is that when the solid is shocked to volumes in the vicinity of the peak, the temperature along the Hugoniot (see Fig. 16) is sufficiently high, that the size of the peak is dramatically reduced.

The Lindemann law[33] for the melting temperature T_m within the Slater model is just $T_m \sim VB_{T,\mathrm{SL}}(V,T_m) \sim VB_{T,\mathrm{SL}}(V,0)$. When normalized to measurements[34] of $T_m(P)$ for fcc La between 20 and 40 kbars, T_m is found to be a monotonically increasing function in P. We find melting to occur along the Hugoniot at $V/V_0=0.61$, $T_H=0.27$ eV, and $P_H=360$ kbars. Since this lies in the region where the stiffening in the u_s-u_p curve begins, there may well be a discontinuous change in slope due to the melting transition. However, the detection of melting in Hugoniot PV or u_s-u_p data has been an elusive quest, and our main contention is that *the overall features of the u_s-u_p curve in La can be explained without invoking the melting transition.* Scaling law analysis[35] suggests that beyond a region of about 3% extent in V/V_0 during which the shocked material is in a two-phase state, the integral Grüneisen parameter, $V\Delta P/\Delta E$, is nearly the same for solid and liquid up to temperatures perhaps a factor of 4 above the melting temperature. Since we estimate $T_m \sim 1.2$ eV at $V/V_0=0.4$, we do not anticipate significant liquid corrections to the present calculations.

ACKNOWLEDGMENTS

We would like to thank R. Grover for suggesting the expression in Eq. (19) and for his comments on liquid corrections. Part of this work was performed under the auspices of the U. S. DOE by Lawrence Livermore National Laboratory under Contract No. W-7405-Eng-48. The work of one of us (H.L.S.) has been supported by the Danish Natural Science Research Council.

[1] O. K. Andersen, Phys. Rev. B 12, 3060 (1975); O. K. Andersen and O. Jepsen, Physica 91B, 317 (1977).
[2] J. C. Slater, *Introduction to Chemical Physics* (McGraw-Hill, New York, 1939) Chaps. XIII and XIV; L. D. Landau and K. P. Stanyukovich, Dokl. Akad. Nauk SSSR, 46, 399 (1945).
[3] L. V. Al'tshuler, A. A. Bakanova, and I. P. Dudoladov, Zh. Eksp. Teor. Fiz. Pis'ma Red. 3, 483 (1966) [JETP Lett. 3, 315 (1966)]; L. V. Al'tshuler, A. A. Bakanov, and I. P. Dudoladov, Zh. Eksp. Teor. Fiz. 53, (1967) [Sov. Phys.—JETP 26, 1115 (1968)].
[4] L. V. Al'tshuler and A. A. Bakanova, Usp. Fiz. Nauk. 96, 193 (1968) [Sov. Phys—Uspekhi 11, 678 (1969)].
[5] W. H. Gust and E. B. Royce, Phys. Rev. B 8, 3595 (1973).
[6] W. J. Carter, J. N. Fritz, S. P. Marsh, and R. G. McQueen, J. Phys. Chem. Solids 36, 741 (1975).
[7] R. Grover and B. J. Alder, J. Phys. Chem. Solids 35, 753 (1974).
[8] D. B. McWhan, G. Parisot, and D. Bloch, J. Phys. F 4, L69 (1974).
[9] D. Glötzel and A. K. McMahan, Phys. Rev. B 20, 3210 (1979).
[10] A. K. McMahan, Phys. Rev. B 17, 1521 (1978).
[11] M. S. Andersen, E. J. Gutman, J. R. Packard, and C. A. Swenson, J. Chem. Phys. Solids 30, 1587 (1969).

[12]A core band will begin to broaden in the course of compression when the Wigner-Seitz radius reaches the region where the core-wave-function tail begins to become significant. Owing to orthogonality, valence wave functions for the same angular momentum, but next-highest principal quantum number, have antinodes near where the core tail starts to become large. As the Wigner-Seitz radius passes inside such antinodes, Wigner-Seitz boundary conditions show that the valence band as a whole begins to move upward relative to the atomiclike energy obtained for the $\varphi(\infty)=0$ boundary condition.

[13]A. Jayaraman, R. C. Newton, and J. M. McDonough, Phys. Rev. 159, 527 (1967).

[14]D. Glötzel, J. Phys. F 8, L163 (1978); D. Glötzel and L. Fritsche, Phys. Status Solidi B 79, 85 (1977).

[15]W. E. Pickett, A. J. Freeman, and D. D. Koelling, Phys. Rev. B 22, 2695 (1980).

[16]C. Probst and J. Wittig, in *Handbook on The Physics and Chemistry of Rare Earths*, edited by K. A. Gschneidner, Jr. and L. Eyring (North-Holland, Amsterdam, 1978), Vol. I, Chap. 10, p. 749.

[17]U. von Barth and L. Hedin, J. Phys. C 5, 1629 (1972).

[18]D. Glötzel and O. K. Andersen, J. Phys. F (in press). The ASA approximation central to the LMTO method may be derived from the usual muffin-tin formalism by requiring the wave functions to have zero kinetic energy in the interstitial region, and then by replacing the muffin-tin radius by the Wigner-Seitz radius in all equations. When this replacement is made in the muffin-tin Madelung term in the total energy [last term in Eq. (14) of J. F. Janak, Phys. Rev. B 9, 3985 (1974)], and the interstitial charge density is taken to be that at the Wigner-Seitz radius, one obtains the muffin-tin correction of Glötzel and Andersen.

[19]A. R. Williams, J. Kubler, and C. D. Gelatt, Jr., Phys. Rev. B 19, 6094 (1979).

[20]A. K. McMahan and M. Ross, Phys. Rev. B 15, 718 (1977).

[21]D. G. Pettifor, Commun. Phys. 1, 141 (1976); D. A. Liberman, Phys. Rev. B 3, 2081 (1971); R. M. Nieminen and C. H. Hodges, J. Phys. F 6, 573 (1976).

[22]Twenty-five pressures, P_i, were calculated along an equally spaced Wigner-Seitz radius grid, S_i, of interval 0.05 bohr. The bulk modulus at $S_{av}=(S_{i+1}+S_i)/2$ was numerically evaluated as $-(S_{av}/3)(P_{i+1}-P_i)/(S_{i+1}-S_i)$.

[23]See Ref. 10. Another small source of scatter has been smoothed in obtaining the results shown in Fig. 2. As volume is reduced, the optimal potential parameter fit to the valence p logarithmic derivative changes character at $V/V_0=0.51$ as the $5p$ band replaces the $6p$ band as the closest nearby p band to the occupied valence states. To test for the uncertainties in this switch, two sets of pressures were calculated at four volumes between $V/V_0=0.47$ and 0.55 according to the two modes for the p potential parameters. The resultant pressures agreed to within about 3%, and the corresponding numerical bulk moduli to about 4%. Thus this uncertainty is quite small, and has no affect on the structure discussed in Fig. 2.

[24]K. Syassen and W. B. Holzapfel, Solid State Commun. 16, 533 (1975).

[25]O. K. Andersen, J. Madsen, U. K. Poulsen, O. Jepsen, and J. Kollar, Physica 86—88b, 249 (1977); A. R. Mackintosh and O. K. Andersen in *Electrons at the Fermi Surface*, edited by M. Springford (Cambridge University Press, Cambridge, 1980).

[26]I. M. Lifshitz, Zh. Eksp. Teor. Fiz. 38, 1569 (1960) [Sov. Phys.—JETP 11, 1130 (1960)].

[27]L. Dagens, J. Phys. (Paris) Lett. 37, 137 (1976); J. Phys. F 8, 2093 (1978).

[28]G. Leibfried and W. Ludwig, in *Solid State Physics*, edited by H. Ehrenreich, F. Seitz, and D. Turnbull (Academic, New York, 1961), Vol. 12, p. 275.

[29]R. M. More, Lawrence Livermore National Laboratory Report No. UCRL-84379 (unpublished); R. Grover, Private communication.

[30]E. B. Royce, in *Physics of High Energy Density*, edited by P. Calderola and H. Knopfel (Academic, New York, 1971), p. 84; V. N. Zharkov and V. A. Kalinin, *Equation of State for Solids at High Pressure and Temperature*, (Consultants Bureau, New York, 1971).

[31]K. A. Gschneidner, Jr., in *Solid State Physics*, edited by H. Ehrenreich, F. Seitz, and D. Turnbull (Academic, New York, 1964), Vol. 16, p. 275.

[32]J. Donohue, *The Structures of the Elements*, (Wiley, New York, 1974).

[33]J. M. Ziman, *Principles of the Theory of Solids*, (Cambridge University Press, Cambridge, 1964).

[34]A. Jayaraman, Phys. Rev. 139, A690 (1965).

[35]R. Grover, J. Chem. Phys. 55, 3435 (1971); and in *Proceedings of the Seventh Symposium on Thermophysical Properties*, edited by A. Cezariliyan (ASME, New York, 1977), p. 67.